JGR Earth Surface

RESEARCH ARTICLE
10.1029/2019JF005252

Sensitivity of the Northeast Greenland Ice Stream to Geothermal Heat

S. Smith-Johnsen[1], N.-J. Schlegel[2], B. de Fleurian[1], and K. H. Nisancioglu[1,3]

[1]Department of Earth Science, University of Bergen, and Bjerknes Centre for Climate Research, Bergen, Norway, [2]Jet Propulsion Laboratory, California Institute of Technology, Pasadena, CA, USA, [3]Centre for Earth Evolution and Dynamics, University of Oslo, Oslo, Norway

Key Points:
- Effective pressure accounts for a substantial part of the spatial variation in NEGIS velocities
- Geothermal heat flux dictates the area and efficiency of the subglacial hydrology system of NEGIS
- Ice flux uncertainty from uncertainties in GHF increases tenfold when effective pressure is considered

Supporting Information:
- Supporting Information S1

Correspondence to:
S. Smith-Johnsen,
silje.johnsen@uib.no

Citation:
Smith-Johnsen, S., Schlegel, N.-J., de Fleurian, B., & Nisancioglu, K. H. (2020). Sensitivity of the Northeast Greenland Ice Stream to geothermal heat. *Journal of Geophysical Research: Earth Surface*, *125*, e2019JF005252. https://doi.org/10.1029/2019JF005252

Received 9 JUL 2019
Accepted 16 DEC 2019
Accepted article online 20 DEC 2019

Abstract Recent observations of ice flow surface velocities have helped improve our understanding of basal processes on Greenland and Antarctica, though these processes still constitute some of the largest uncertainties driving ice flow change today. The Northeast Greenland Ice Stream is driven largely by basal sliding, believed to be related to subglacial hydrology and the availability of heat. Characterization of the uncertainties associated with Northeast Greenland Ice Stream is crucial for constraining Greenland's potential contribution to sea level rise in the upcoming centuries. Here, we expand upon past work using the Ice Sheet System Model to quantify the uncertainties in models of the ice flow in the Northeast Greenland Ice Stream by perturbing the geothermal heat flux. Utilizing a subglacial hydrology model simulating sliding beneath the Greenland Ice Sheet, we investigate the sensitivity of the Northeast Greenland Ice Stream ice flow to various estimates of geothermal heat flux, and implications of basal heat flux uncertainties on modeling the hydrological processes beneath Greenland's major ice stream. We find that the uncertainty due to sliding at the bed is 10 times greater than the uncertainty associated with internal ice viscosity. Geothermal heat flux dictates the size of the area of the subglacial drainage system and its efficiency. The uncertainty of ice discharge from the Northeast Greenland Ice Stream to the ocean due to uncertainties in the geothermal heat flux is estimated at 2.10 Gt/yr. This highlights the urgency in obtaining better constraints on the highly uncertain subglacial hydrology parameters.

1. Introduction

The Greenland Ice Sheet (GrIS) holds the equivalent of more than 7 m of sea level rise (Church et al., 2013), and the loss of mass has accelerated in recent decades (van den Broeke et al., 2009). Numerical ice sheet models are critical tools in predicting the response of the GrIS to a warming climate, and thus estimating its contribution to future sea level rise. The current predictions of sea level rise cover a large range of values (4.5–66.3 cm the next century; Bindschadler et al., 2013), partly due to uncertainties within the ice sheet models as a result of simplified representations of physical processes, and partly associated with errors in the boundary conditions.

Initial conditions such as the ice front position, surface velocity, and elevation can be observed directly or remotely and are relatively well constrained. The basal regime, on the other hand, is less understood and poorly represented in ice sheet models, with temperatures being one of the least constrained parameters (Seroussi et al., 2013). The temperature of the ice controls the softness and its internal deformation (Glen, 1955), in addition to controlling where the base of the ice sheet is frozen and where it is sliding over the bed. Geothermal heat flux (GHF) is an important boundary condition in the thermal component of ice sheet models, controlling the basal temperatures and therefore basal melt rates and ice flow. Unfortunately, the magnitude and spatial variation of the GHF under the GrIS is largely unknown (Rogozhina et al., 2012) and observations are limited to a few point measurements from deep drilling sites (GRIP, 1993; NGRIP, 2004; NEEM, 2013).

Our study area, the Northeast Greenland Ice Stream (NEGIS), drains 12% of the area of the GrIS (Rignot & Mouginot, 2012) and is thus a major contributor to the mass balance of the ice sheet. This highly dynamic region is particularly interesting as it has been suggested that the ice stream is initiated by a GHF anomaly (Fahnestock et al., 2001), resulting from the passing of Greenland over the Icelandic hot spot between 80 and

35 million years ago (Doubrovine et al., 2012; Rogozhina et al., 2016; Storey et al., 2007). GHF models for this region show a large spread, both in spatial distribution and magnitude of the heat flux (Martos et al., 2018; Rogozhina et al., 2012). The spread is caused by different methods in retrieving the GHF, varying between tectonic (Pollack et al., 1993), seismic (Shapiro & Ritzwoller, 2004), magnetic (Fox Maule et al., 2009; Martos et al., 2018), or one of the three previous methods in combination with an ice sheet model (Greve, 2019; Rogozhina et al., 2016). A broad GHF range leads to a large disparity in the thermal boundary conditions for dynamical ice sheet models. Our goal is to quantify the influence of the uncertainty in the GHF on the estimated ice flux from the NEGIS.

One approach to assess the influence of input uncertainties, and how they propagate through numerical models, is through uncertainty quantification (UQ). UQ has previously been used in ice sheet models for both Greenland and Antarctica (Larour et al., 2012; Schlegel et al., 2013, 2015, 2018) as provided by the Ice Sheet System Model (ISSM) (Larour et al., 2012). Larour et al. (2012) used UQ to investigate the impact of errors in GHF for Pine Island Glacier, West Antarctica, and concluded that the influence is small in fast-flowing areas, relative to initial thickness and basal drag. Similarly, Seroussi et al. (2013) showed how a model of the GrIS was far more sensitive to variations in basal drag than initial temperature. Schlegel et al., 2013 (2013, 2015) utilized UQ tools for the NEGIS region investigating how errors in surface mass balance (SMB), basal drag, and GHF influenced a forward simulation on decadal time scales. They also concluded that the impact of geothermal heat was small relative to basal drag and SMB.

We expect that the sensitivity of ice dynamics to the GHF is enhanced when including subglacial hydrology in the model, as the basal drag responds to changes in basal water supply. Here we build upon the work by Schlegel et al. (2015) and investigate the sensitivity of the ice flow to basal conditions. We improve the sampling study of mass flux uncertainty by including a subglacial hydrology model (de Fleurian et al., 2014, 2016).

Our aim is to quantify ice flow uncertainties in a decadal-scale forward simulation of the NEGIS, including uncertainties in the GHF. Furthermore, we will disentangle the uncertainty resulting from uncertainties in viscosity and sliding and compare these to mass flux uncertainties associated with uncertainties in SMB.

2. Methods

To simulate the ice flow of the NEGIS, we use the ISSM, a three-dimensional thermomechanical finite element model with an adaptive anisotropic mesh. This study builds upon the work by Schlegel et al., 2013 (2013, 2015) by focusing on the impact of the GHF. We expand upon these previous studies by utilizing a wide range of GHF maps and including a coupled subglacial hydrology model to capture the dynamic effect of variations in the basal melt. First, we describe the relevant components of the ice flow model, then we describe how we adapted the continental Greenland model from Schlegel et al. (2016) and extracted our model domain, and finally we describe the UQ analysis.

2.1. Ice Sheet Model

The ISSM conserves mass, and ice thickness evolves through time following the mass transport equation, relating the rate of ice thickness change to the divergence of ice flow, SMB, and basal mass balance:

$$\frac{\partial H}{\partial t} = \dot{M}_s + \dot{M}_b - \nabla \cdot H\bar{v} \tag{1}$$

where $\dot{M}_s$ is the SMB, $\dot{M}_b$ is the basal mass balance, and $\bar{v}$ is the depth-averaged horizontal velocity. For bedrock geometry we use "Bedmachine" (Morlighem et al., 2014) gridded at 150-m resolution and interpolated to our mesh. The initial ice surface data is taken from Howat et al. (2014). At the floating ice shelves we apply submarine melt rates from Rignot et al. (2001). To calculate the temporal evolution of the three-dimensional ice temperature and basal melt rates, we rely on the enthalpy formulation (Aschwanden et al., 2012), validated in ISSM by Seroussi et al. (2013). This thermal model accounts for horizontal and vertical advection, diffusion, viscous heating, GHF, and frictional heating. We apply a Dirichlet boundary condition at the surface using temperatures from Ettema et al. (2009). The following Neumann boundary condition is applied at the base:

$$k_{th}\ \nabla T \cdot \mathbf{n} = G - \tau_b \cdot \mathbf{v}_b \tag{2}$$

The left side of the equation is the heat flux applied at the glacier bed, where k_{th} is ice thermal conductivity, ∇T the temperature gradient and $\mathbf{n}$ the normal vector to the ice bed interface. The right side is the GHF, G, and the frictional heat computed as the product of the basal velocity, $\mathbf{v}_b$, and basal drag, τ_b.

Ice is treated as an incompressible material with viscosity, μ, following Glens flow law (Glen, 1955):

$$\mu = \frac{B}{2\dot{\epsilon}_e^{\frac{n-1}{n}}} \tag{3}$$

where B is the ice viscosity parameter varying with depth, $n = 3$ is Glen's flow law exponent, and $\dot{\epsilon}_e$ is the effective strain rate. B is temperature dependent following the Arrhenius relation:

$$B = B_0 \quad exp\left(-\frac{Q^-}{RT_h}\right) \tag{4}$$

where the coefficient B_0 is a prefactor, Q^- is the activation energy for creep, R is the gas constant, and T_0 is pressure corrected temperature of ice (Cuffey & Paterson, 2010).

For calculating the stress balance we apply the hybrid L1L2 scheme (Hindmarsh, 2004) as an approximation to the Stokes equations. At the surface we apply a Neuman boundary condition with zero air pressure, and hydrostatic water pressure at the ice front. We use a standard linear friction law (Cuffey & Paterson, 2010), linking basal shear stress to basal velocity:

$$\tau_b = -\alpha^2 N \mathbf{v}_b \tag{5}$$

where α is the basal drag coefficient. To retrieve α, we rely on the powerful inversion tool in ISSM to best match observed surface velocities. N is the effective pressure, the difference between overburden pressure, P_i, and water pressure at the bed, P_w. Commonly, effective pressure is approximated to the hydrostatic pressure, $N = g(\rho_i H + \rho_w z_b)$, where ρ_i and ρ_w are density of ice and water respectively, and z_b is bed elevation relative to sea level and negative below sea level.

Here, on the other hand, we compute the effective pressure, using a one-way coupling with a subglacial hydrology model (de Fleurian et al., 2014, 2016), designed for large-scale studies. The model consists of two porous sediment layers, representing the inefficient and efficient drainage system. The source of the inefficient drainage system is basal melt only. The source of the efficient drainage is a transfer term between the two layers where the flux is driven by differences in water head between the two drainage systems. The efficient drainage system may activate and deactivate in regions where effective pressure reaches 0, and the thickness of the layer evolves similarly to how the size of subglacial channels evolve. The efficient drainage system will be deactivated if the thickness reaches a minimum value. To compute the effective pressure, the pressure of the inefficient drainage system is used.

The hydrology model is coupled to the thermomechanical ice flow model by taking the basal melt rates as input and computing the effective pressure in the friction law (equation (5)). The frozen nodes in the model domain have effective pressure set equal to the ice overburden pressure, P_i. The hydrology model demands a smaller time step than the ice flow model, and we use a monthly resolution for the ice flow model and 6-hourly resolution for the hydrology model. The hydrology model is described in detail in de Fleurian et al. (2014, 2016).

2.2. Model Forcing and Relaxation

Here we adopt the continental Greenland model from Schlegel et al. (2016) where the surface is forced with a constant SMB value derived from the mean over the period from 1979–1988 (Box, 2013), when Greenland's total mass balance was close to 0, hereafter referred to as ISSM-GrIS. ISSM-GrIS has two layers, and we extrude the model to give vertical layers. In order to get a new thermal regime consistent with the new model state and boundary conditions for our regional model, we run a thermal steady-state simulation for the continental model, ISSM-GrIS-SS. From ISSM-GrIS we extract a regional model over the NEGIS, setting boundary conditions after the methods described in Schlegel et al. (2013, 2015), and we name the resulting model ISSM-NEGIS. Velocity and thickness boundary conditions for all ice-ice boundaries in ISSM-NEGIS come from ISSM-GrIS (Schlegel et al., 2016), while thermal boundary conditions come from ISSM-GRIS-SS. With the new boundary conditions for ISSM-NEGIS we first run a steady-state simulation, and then relax the model for 1 kyr to reach equilibrium.

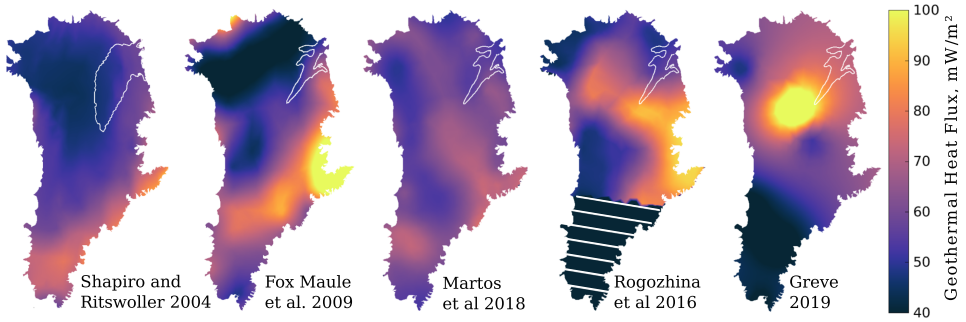

Figure 1. The five geothermal heat flux data sets for Greenland used in this study. The white contour in the map by Shapiro and Ritzwoller (2004) shows the model domain, and in the remaining maps the white contour outlines the 50-m/yr ice surface velocity for the Northeast Greenland Ice Stream (NEGIS). Straight white lines in the map by Rogozhina et al. (2016) indicate an area with no model data.

The ISSM-NEGIS model domain stretches from the ice divide to the floating shelves of 79°N and Zachariæ outlets, see Figure 1. The domain is discretized into 9,974 horizontal elements, ranging from 1 km in areas with high-velocity gradients and to a maximum of 15 km at the ice divide. The horizontal mesh is extruded to five vertical layers resulting in a total of 49,870 prismatic elements. We use linear P1 elements for the stress balance analysis and quadratic P2 elements for the thermal analysis. The P1P2 elements have been tested and validated in ISSM by Cuzzone et al. (2018) and allow us to capture sharp thermal gradients, despite having only five layers.

We investigate five GHF distribution maps for Greenland and use Martos et al. (2018) as our reference map in the model (Figure 1). First, we take ISSM-NEGIS and run a thermal steady state to retrieve basal melt rates, which serves as input to the hydrology model. The hydrology model computes effective pressure for use in the sliding law (equation (5)). As we alter the effective pressure, the α from ISSM-NEGIS is no longer valid and we do another inversion to best match observed velocities. Finally, we relax the model for 7 kyr to make sure a new equilibrium is reached. This second relaxation is longer, as the ice flow model needs more time to equilibrate after a change in basal drag relative to a change in temperature. This model, ISSM-NEGIS-hydro, becomes the initial state for the main simulation, in which we investigate how GHF influences mass flux through the ice stream. The simulation lasts 23 yr, and we force the model with monthly SMB from the Year 1981 to 2011 after Box (2013), with modifications described in Schlegel et al. (2016) supplementary. Temperature is forced through time with yearly means from Box (2013). Both effective pressure and α are being held fixed in time, while ice viscosity can change through time as ice temperature evolves. We refer to this final simulation as ISSM-NEGIS-transient.

2.3. UQ

To investigate how uncertainties in GHF propagate forward in the model and impact the NEGIS ice flow, we use the UQ framework Dakota (Design Analysis Kit for Optimization and Terascale Applications; Eldred et al., 2008; Swiler & Wyss, 2004) embedded in ISSM. Dakota takes interval information on model inputs, like geothermal heat, and maps them through the model by running the same simulation many times in a Monte Carlo style. This is a nondeterministic analysis, where a model field is perturbed by a different amount for each simulation: resulting in a range of model output used to assess statistics on model diagnostics. During the analysis, we use mass flux through gates across critical areas within the ice stream as the diagnostics. Dakota produces a statistical distribution for each of the flux gates and calculates the mean ice flux, standard deviation, and cumulative distribution functions. Finally, we define model uncertainty as the total range at each statistical distribution of the mass flux at each gate. Usage and implementation of Dakota in ISSM is described in detail in (Larour et al., 2012; Schlegel et al., 2013).

The five GHF maps for Greenland (Figure 1) form the basis to define uncertainty bounds used in two sampling experiments; one testing the mass flux uncertainty to ice viscosity, B, and one testing the mass flux uncertainty to effective pressure, N. For each node in the model we find the maximum and minimum values among all the five GHF maps and produce a minimum and maximum composite map (Figures 4b and 4c). This means that the resulting minimum a maximum maps consist of GHF values from several of the

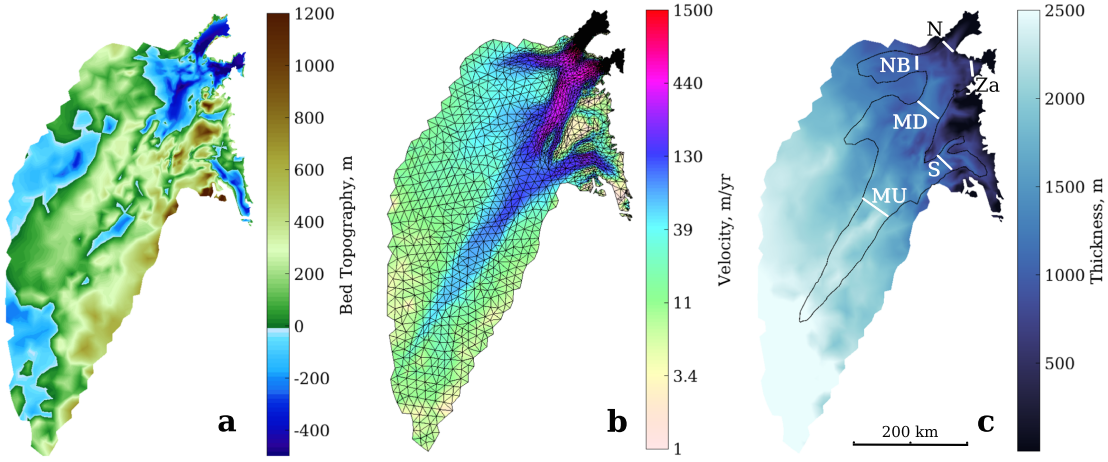

Figure 2. (a) Bed topography after Bedmachine (Morlighem et al., 2014) interpolated onto the model grid, (b) observed surface velocity (Rignot & Mouginot, 2012) and model mesh, and (c) ice thickness and flux gates used in the uncertainty quantification.

published GHF maps in Figure 1 and allows us to capture the full spread of GHF values used in ice sheet models.

For each map we run a thermal steady-state solution to retrieve the corresponding viscosity parameter and basal melt rates. The viscosity parameter (B in equation (3)), for the maximum and minimum GHF, serves as upper and lower bounds in the uncertainty distribution in the first sampling analysis; viscosity sampling analysis (Figures 4e and 4f). The model includes five vertical layers, and we derive viscosity uncertainties based on Layer 2, directly above the basal layer as the Dakota framework only allows 2-D sampling. The entire ice column is perturbed by the uncertainties from Layer 2, and we believe this represents a middle value, because Layer 2 considers basal and interior ice values. For this experiment we turn off the thermal model, as the ice viscosity comes from the steady-state model (ISSM-NEGIS-Hydro) and is perturbed by the sampling analysis.

The basal melt rates for the maximum and minimum GHF are used to calculate the effective pressure distribution for the two extreme cases, which serves as upper and lower uncertainty bounds for our second sampling experiment: effective pressure sampling (Figures 4j and 4l). For comparison, we also run an updated SMB UQ similar to Schlegel et al. (2013); "SMB sampling" analysis. See supporting information for details on this updated component-based SMB error sampling (Schlegel & Larour, 2019).

As the model mesh is anisotropic, we divide the model domain into 1,000 partitions of equal area, using "Chaco" (Software for Partitioning Graphs; Hendrickson & Leland, 1995). The large variation in element size leads to a variation in how many ISSM mesh vertices are assigned to each partition. Both viscosity and effective pressure uncertainties are described as a statistical uniform distribution for each partition, which means that the probability of occurrence is equal for any given value within the interval.

We use the six flux gates across the ice stream following Schlegel et al. (2015): one across each of the major outlets 79North (Gate N), Zachariæ Isstrøm (Gate Za), and Storstrømmen (Gate S); one across the northern branch of the NEGIS (Gate NB); and two across the main branch, one downstream (Gate MD) and one upstream (Gate MU) (Figure 2c). Gate Za and N are moved further upstream relative to Schlegel et al. (2015), as we include grounding lines and floating ice tongues in the current model setup.

Finally, we carry out the three UQ sampling analyses by running ISSM-NEGIS-transient for 23 yr, described in 2.2. Dakota launches this simulation 388 times for each of the three sampling analyses and randomly perturbs the sampling field each time. For the viscosity sampling analysis, the ice viscosity is perturbed, in the effective pressure sampling analysis the effective pressure is perturbed, and for comparison, in the "SMB sampling" analysis the surface forcing is perturbed. The viscosity sampling analysis let us investigate how the GHF changes the viscosity of the ice, and the following ice flux through the ice stream. In the effective pressure sampling analysis we look at how the GHF influences the friction at the base, and in this way impacts the ice flux.

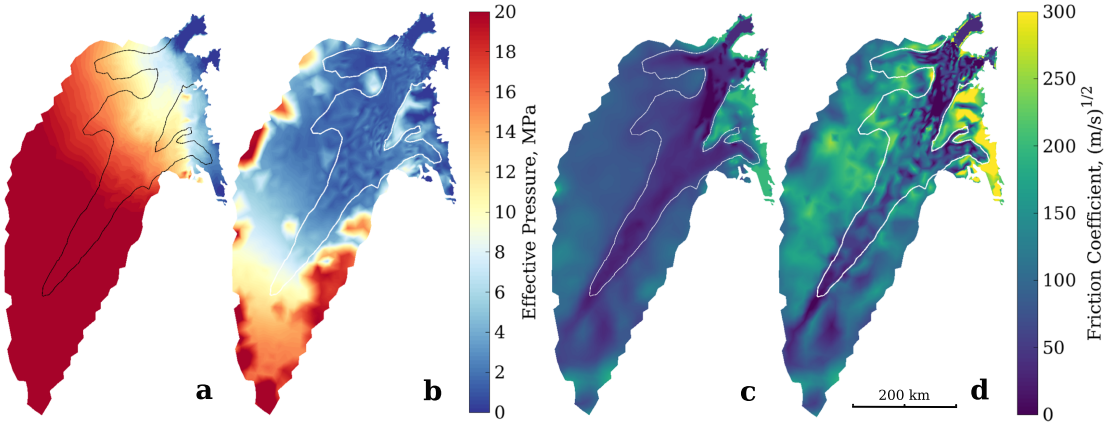

Figure 3. Differences between a model with and without subglacial hydrology. (a) Approximated effective pressure using hydrostatic pressure in ISSM-NEGIS, (b) modeled effective pressure from the hydrology model in ISSM-NEGIS-hydro, (c) inversion results for friction coefficient in ISSM-NEGIS, and (d) inversion results for friction coefficient for ISSM-NEGIS-hydro. Black and white contours indicate 50 m/yr observed surface velocity.

3. Results

The goal of this study is to quantify the uncertainty in ice flux through the NEGIS Schlegel et al. (2013, 2015). We focus on uncertainties in the GHF and investigate how these propagate through the model by impacting the ice viscosity and basal drag.

Figure 3 summarizes the differences between a model with and without a hydrology model, that is, comparing ISSM-NEGIS and ISSM-NEGIS-hydro. Most ISSM simulations use hydrostatic pressure with perfect connectivity to the ocean to calculate an approximation of effective pressure, shown in Figure 3a for ISSM-NEGIS. Inverting for the basal friction coefficient (α) using observed surface velocities, gives a pattern with low values within the ice stream and higher outside, see Figure 3c. For this study, we model effective pressure using a subglacial hydrology model.

The effective pressure computed in ISSM-NEGIS-hydro suggests that when considering heat flux, most of the domain is thawed, and only the boundaries upstream are frozen. The effective pressure of these frozen regions is set equal to the ice overburden pressure. The spatial distribution of α obtained from the inversion in ISSM-NEGIS-hydro, using the modeled effective pressure in the friction law, is shown in Figure 3d. The modeled effective pressure distribution shows generally lower values than that approximated using only the hydrostatic pressure (Figure 3a), and thus, the new inversion compensates for this by estimating higher values for the friction coefficient. Particularly high α values are reached outside the ice stream (white contour in Figure 3), where both the observed velocities and modeled effective pressures are low. Close to the grounding line both the modeled and approximated effective pressure show low values, and hence, α distributions are similar in this region (Figures 3c and 3d). A region downstream of gate MD (Figure 2c) shows very low α values for both inversions, and correlates with a deep bed topography below sea level (Figure 2a).

3.1. Sampling Uncertainties

Figure 4 presents the initial state for the 23-yr simulation (first column) and the uncertainty bounds for various parameters caused by minimum GHF (second column) or maximum GHF (third column) using the ISSM-NEGIS-hydro model. The minimum GHF map (Figure 4b) consists of data from Rogozhina et al. (2016), Shapiro and Ritzwoller (2004), and Fox Maule et al. (2009) combined. The maximum GHF values (Figure 4c) mostly consist of values from Greve (2019), see Figure 1. The differences between the two extreme GHF are largest in the southwest region and show up to 256% change. The reference GHF (Martos et al., 2018) is closer in magnitude to the minimum than the maximum map. The ice temperatures from the minimum and maximum GHF, and the corresponding ice viscosity parameter are shown in Figures 4e and 4f, respectively. The minimum and maximum viscosity parameter fields are used as lower and upper uncertainty bounds in the viscosity sampling experiment. Generally, we find low values of the ice viscosity in the shear margins and where the velocity gradients are the highest. We observe softer ice (i.e., lower values of B) in the maximum GHF case relative to the minimum GHF case, as expected with higher ice temperatures.

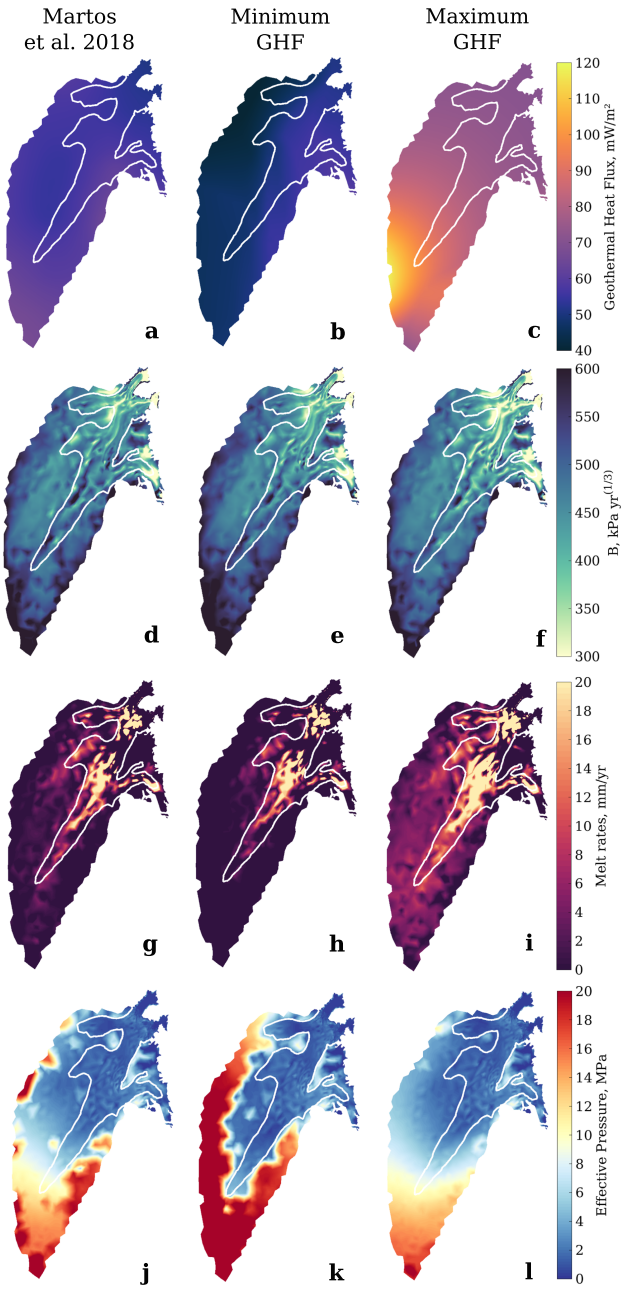

Figure 4. Reference geothermal heat flux (GHF, mW/m^2) with corresponding parameters for the initial state in ISSM-NEGIS-transient (first column), with uncertainty bounds as a result of minimum (second column) and maximum (third column) GHF. The first row shows the reference (a), minimum (b), and maximum (c) geothermal heat fluxes. The second row (d–f) shows the corresponding ice viscosity parameter *B* for Layer 2 used in viscosity sampling. The third row (g–i) shows the corresponding basal melt rates, and the last row (j–l) shows the corresponding effective pressure used in effective pressure sampling.

The steady-state solutions for ISSM-NEGIS-hydro forced by the minimum and maximum GHF provide basal melt rates, shown in Figures 4h and 4i, respectively. The associated basal melt rates for the GHF minimum map show positive values within the main trunk of the ice stream, where velocities are around 50 m/yr and higher, indicating the importance of frictional heat. A large part of the domain is frozen in the minimum GHF distribution, as opposed to the maximum GHF where most of the domain reaches the pressure melting point also outside the ice stream. Basal melt rates within the ice stream also increase, indicating that a

change in GHF does impact the basal thermal regime, also in fast-flowing areas, despite frictional heat being the dominant heat source here. The region around gate MU shows no melting for either of the GHF distributions, despite being in a high-velocity region.

The basal melt rates force a subglacial hydrology model that computes effective pressure. In Figure 4 we show the effective pressure maps computed for both the minimum (Figure 4k) and the maximum (Figure 4l) GHF. These minimum and maximum effective pressure fields are used as lower and upper uncertainty bounds in the effective pressure sampling experiment. Here it is clear to see that for the minimum case a large part of the domain outside the ice stream is frozen to the bed and displaying high effective pressure. This is not the case for the maximum GHF map, where the hydrology model is activated for most of the domain.

Within the ice stream the two effective pressure fields are similar. We observe lower effective pressure upstream for the minimum GHF than for the maximum and reference, which may be counter intuitive. Despite lower basal melt rates for the minimum case, implying less meltwater, the water has a smaller region to spread out on, and thus, effective pressure remains low. More details on the hydrology simulations for the three GHF maps are provided in supporting information Figure S1 and Table S1.

3.2. Sampling Analysis

We present results from all three sampling analyses in the relative frequency histograms in Figure 5. Each histogram represents the range and frequency of ice flux for the six flux gates at the end of the 388 simulations, with results from the viscosity sampling (black), effective pressure sampling (blue) and SMB sampling (green). We define the uncertainty as the total range of mass flux for each distribution (Δ Mf). Sampling statistics for each flux gate for the three sampling analyses are summarized in Table 1 showing the mean flux (μ), minimum and maximum 95% percentile, standard deviation (σ), and the total mass flux range (Δ Mf). The ΔMf/ref shows the value range in percent where "ref" is the mass flux value from the reference simulation, that is, without any model field perturbations. We also include the total NEGIS flux uncertainty as the sum of the three outlets: Zachariæ, 79North, and Storstrømmen (Za, N, and S in Figure 2c).

All histograms from the six flux gates display normal distributions with small skew values (Table S2), despite the input forcing being uniformly distributed, indicating a sufficient number of samples. The mean mass fluxes for each gate varies between the experiments. All the distributions are centered at zero for a clearer comparison. We observe that for most flux gates in Table 1, the reference mass flux is smaller than the means from the three sampling analyses, apart from gate NB and Za in the SMB sampling. The reason for this shift in mean mass flux values is that the reference GHF by Martos et al. (2018) is lower than the average between minimum and maximum GHF. As we sample uniformly the means will be shifted toward higher values, leading to softer ice and more basal lubrication, hence higher mass flux through the gates. Effective pressure has a more direct impact on ice velocity than the viscosity parameter, and thus, the means are shifted toward higher mass fluxes in the effective pressure sampling.

Generally, we find that the viscosity sampling gives smaller mass flux uncertainty than the effective pressure sampling for all the flux gates, on average by a factor 10. The largest difference between viscosity and effective pressure is found in gate MU with a viscosity uncertainty 30 times smaller than for the effective pressure. The ice flux uncertainty for this gate is the smallest for both the viscosity and SMB, but at the same time it shows one of the largest uncertainties in the effective pressure sampling. The effective pressure uncertainty is generally the same order of magnitude as the SMB uncertainty (Table 1), and larger than SMB for three out of six gates.

The smallest uncertainty in the viscosity sampling is in a region with slow velocity, and the largest uncertainties are in the fast-flowing outlets (N and Za) and the Northern Branch (NB) where strain rates are high. We derive uncertainties of viscosity in the layer directly above the basal layer, and viscous heating and softening are more intense in regions with high-velocity gradients. N is the most sensitive gate for the viscosity sampling, in agreement with Schlegel et al. (2015). This is where we observe the largest difference between GHF max and min, leading to the most softening. The smallest uncertainty in the effective pressure sampling is found at gate MD. This is a region where melt input is 0 for all cases, due to low basal friction as ice flows over the overdeepened bed. On the other hand, MD shows the highest uncertainty in the SMB sampling. The largest uncertainty in effective pressure sampling is gate NB; an area with both large GHF uncertainties and a close proximity to regions that shift from frozen to thawed between min and max GHF.

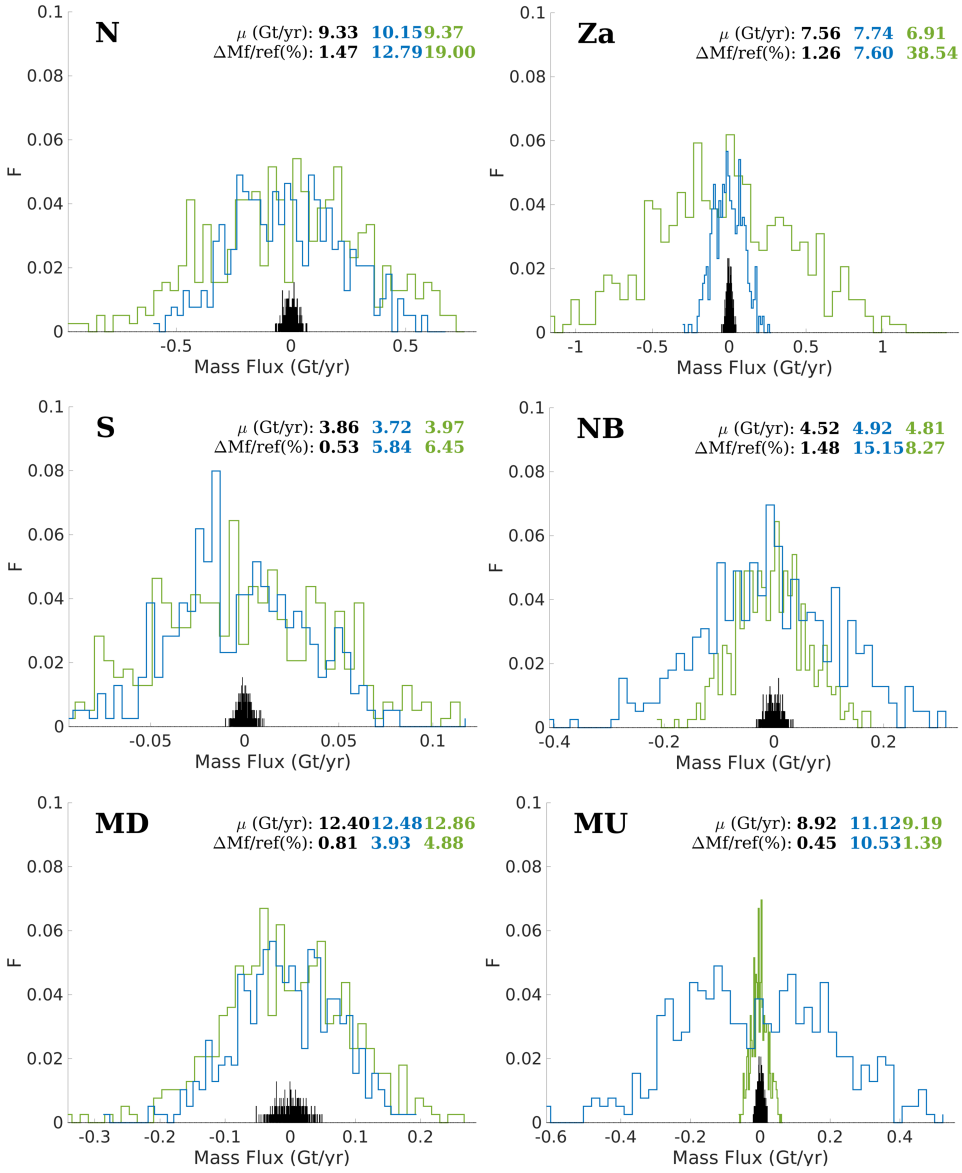

Figure 5. Statistical distributions of mass flux frequency and range, at the end of 388 simulations for each of the six flux gates in Figure 2c, resulting from uncertainties in the ice viscosity parameter *B* (black), effective pressure, *N* (blue), and surface mass balance, SMB (green).

Overall, we find that the uncertainty associated with effective pressure uncertainties are significantly larger than those associated with uncertainties in ice viscosity. Both analysis show ice flux uncertainty due to the uncertainty in the GHF. However, the effective pressure analysis includes the hydrological effect on sliding, and thus displays larger ice flux uncertainty as it has a first order impact on ice velocity. The total uncertainty for the NEGIS ice flux due to uncertainties in the GHF, associated with ice viscosity and effective pressure, is 1.23% and 10.26%, respectively. We find that ice viscosity influences downstream mass flux more than upstream. In particular, regions with high-velocity display large mass flux ranges. We do not observe the same pattern for the effective pressure sampling, as we find large uncertainties also upstream.

4. Discussion

Here we investigate how the spread of GHF values used in ice sheet models impact mass transport through the NEGIS. The study expands upon previous work by Schlegel et al. (2015) by using a larger range of GHF

Table 1
Statistics[a] for Sampling Histograms in Figure 5

Variable	Ref	*B*	*N*	SMB
Gate N				
μ	9.22	9.33	10.15	9.37
95% Min		9.29	9.78	8.82
95% Max		9.37	10.57	9.94
σ		0.0244	0.2403	0.3386
ΔMf		0.14	1.30	1.78
ΔMf/ref (%)		1.49	14.09	19.32
Gate Za				
μ	7.45	7.56	7.74	6.91
95% Min		7.53	7.58	6.16
95% Max		7.59	7.89	6.67
σ		0.0164	0.0960	0.4552
ΔMf		0.09	0.59	2.66
ΔMf/ref (%)		1.27	7.90	35.73
Gate NB				
μ	4.50	4.52	4.92	4.81
95% Min		4.50	4.71	4.70
95% Max		4.54	5.12	4.92
σ		0.0128	0.1253	0.0659
ΔMf		0.07	0.675	0.40
ΔMf/ref (%)		1.48	16.56	8.84
Gate MD				
μ	12.27	12.40	12.48	12.86
95% Min		12.37	12.35	12.70
95% Max		12.43	12.60	13.02
σ		0.0180	0.0787	0.0978
ΔMf		0.10	0.49	0.63
ΔMf/ref (%)		0.82	4.00	49.38
Gate S				
μ	3.85	3.86	3.72	3.97
95% Min		3.85	3.67	3.89
95% Max		3.87	3.78	4.05
σ		0.0035	0.0359	0.0476
ΔMf		0.02	0.22	0.26
ΔMf/ref (%)		0.53	6.65	3.91
Gate MU				
μ	8.90	8.92	11.12	9.19
95% Min		8.91	10.79	9.16
95% Max		8.93	11.49	9.24
σ		0.0088	0.2188	0.0236
ΔMf		0.04	1.17	0.13
ΔMf/ref (%)		0.46	13.16	1.44
NEGIS outflux				
μ	20.51	20.75	21.61	20.25
ΔMf		0.25	2.10	4.70
ΔMf/ref (%)		1.23	10.26	22.91

[a]Statistics include the following mean mass flux (μ in Gt/yr), the minimum and maximum mass flux values for the 95th percentile of samples (Gt/yr), the standard deviation of the sampling distribution (μ in Gt/yr), the total range of mass flux values (ΔMf in Gt/yr), and the percent mass flux uncertainty (defined as ΔMf/ref in percent).

and includes a subglacial hydrology model to capture changes in effective pressure and sliding. In earlier GHF sensitivity studies, GHF only influences ice softness (Larour et al., 2012; Schlegel et al., 2015). Here we find that ice flux uncertainties, from uncertainties in the GHF, increase tenfold when including the impact of effective pressure.

We find that for all flux gates, mass flux uncertainty associated with ice viscosity is less than 1.5%. This is in agreement with results from Schlegel et al. (2015), where the authors conclude that the GHF induced ice viscosity variations have little effect on decadal-scale ice flow. Ice flux uncertainty for the main outlets is three times smaller than Schlegel et al. (2015) in the viscosity sampling, despite having a larger uncertainty range. Here we include floating ice shelves; thus, the outlets are thinner and may respond differently to Schlegel et al. (2015). On the other hand, the upstream gates have very similar uncertainties. Larour et al. (2012) investigate how the GHF impacts ice viscosity, and in turn ice flow in Antarctica. They conclude that, in fast-flowing regions of Pine Island Glacier, an error of up to 50 mW/m^2 in GHF leads to a 1% change in the mass flux of the ice stream for a stress balance calculation. We find an uncertainty of 1.23% in mass flux associated with uncertainty in the ice viscosity parameter, in agreement with (Larour et al., 2012; Schlegel et al., 2015).

Here we use a subglacial hydrology model to capture the influence on sliding from a change in basal melt rates when the GHF is varied. For example, an increase in basal melt rates will lower effective pressure which, through the sliding law, enhances the velocity. By sampling both the ice viscosity, and the effective pressure, we find that uncertainty in ice flux is ten times higher for effective pressure relative to ice viscosity, averaged over the six flux gates. For most gates, the effective pressure sampling uncertainty is only slightly smaller than the 20% uncertainty in the friction coefficient α in Schlegel et al. (2015). Thus, we find the GHF to be more important for ice dynamics than previously shown. This also holds in fast-flowing regions, illustrating the importance of accounting for the impact of GHF on effective pressure.

GHF controls the water production, which in turn impacts the effective pressure. The difference in effective pressure between low and high GHF is evident in Figures 4k and 4l, particularly outside the main trunk. The subglacial hydrology model develops an efficient drainage system in the two main outlets and in the overdeepened region around gate MD (Figures S1d–S1f). This is in agreement with Beyer et al. (2018). The floatation fraction (ratio of water pressure over ice pressure) within the main trunk has values higher than 0.8, meaning close to floatation for all three GHF cases (Figures S1g–S1i). The difference in the distribution of the efficient drainage system, between the minimum and the maximum GHF cases, shows that the efficient drainage system develops further upstream toward gate MU given a higher GHF. This explains why we do not observe a significant difference in effective pressure between low and high GHF, within the lower part of the main trunk (Figures 4k and 4l). Instead of increasing the water head in the inefficient system, and thus decreasing the effective pressure, the efficient layer activates and compensates for the increased water input.

The sampling of effective pressure shows high uncertainty for the upstream gate MU, as opposed to the trend in the sampling of the ice viscosity with increasing uncertainty toward the terminus (in agreement with Schlegel et al., 2015). The small uncertainties for the sampling of effective pressure in the outlet gate of Zachariρ, relative to upstream, may be explained by high melt water input to the hydrology model for both low and high GHF. The gate of Zachariρ displays the highest velocities, and therefore the highest melt rates, as a result of frictional heating. High water input leads to an activation of the efficient drainage system, which can accommodate an increase in water input without giving a decrease in the effective pressure. On the other hand, the flux gate upstream (MU) is in a region with a less developed drainage system, with lower water heads, and no efficient drainage system. An increase in water input here will directly increase water heads, and hence lower the effective pressure, leading to higher velocities. This upstream sensitivity is in agreement with Keisling et al. (2014), where they conclude that upstream NEGIS is controlled by water routing, as opposed to the topographic and oceanic control of the downstream part.

The resulting uncertainty in the sampling of effective pressure is assumed to be dependent on the choice of parameters in the hydrology model. In particular, the parameters determining how efficient the system is in evacuating water (transmissivity, conductivity, and layer thickness; Table S1) will influence how sensitive the computed effective pressure is to basal melt rates. For example, we use a transmissivity of $0.002\ m^2/s$ for the inefficient drainage system; however, a system with lower transmissivity would be more sensitive to an increase in water input relative to a system with high transmissivity. One therefore expects a larger

range of effective pressure with the same GHF uncertainties by varying the parameters for the hydrology model, and for this reason we may underestimate the uncertainty. Unfortunately, the parameters relating to the subglacial hydrology are largely unknown due to lack of observations in the inaccessible subglacial environment.

Another underestimation of uncertainty is caused by the short time period of our transient simulation (23 yr). This choice was made to be consistent and to be able to directly compare the uncertainties with those of Schlegel et al. (2013, 2015). Although we capture the full thermal impact of the GHF on viscosity and hydrology as we run steady-state simulations to calculate the uncertainties, we do not capture the full transient mass transport and stress balance response to these perturbations given the short period of time. A shift from frozen to thawed bed, just outside the main trunk, will influence the advection of ice into the ice stream, an important process for the NEGIS (Keisling et al., 2014). Ice in a region with velocities of 50 m/yr will be advected 1 km during the 23-yr period. On the other hand, Schlegel et al. (2015) showed that changes in basal conditions can influence regions 300 km away, as a result of secondary processes for the same time period.

We use five GHF maps to define the uncertainty bounds in the sampling studies, however, GHF values 10 times higher have been suggested for the NEGIS region (Fahnestock et al., 2001). These were not included here, as they are local findings and not spatially distributed maps, and by excluding these high values, we underestimate the ice flux uncertainties. GHF is also thought to be changing in time which would impact the temporal stability of the NEGIS; however, this is beyond the scope of the paper. By using five GHF maps obtained from different methods we lose the spatial variability in the sampling analysis and may end up with unrealistic combinations. This limitation could have been improved by using only one GHF map with corresponding data uncertainty. However, the aim of this study is to investigate the full spread of GHF values used in ice sheet models, and not individual GHF products.

Our findings imply that the GHF dictates the extent and efficiency of the hydrology system for the NEGIS. As the GHF determines where the bed is frozen, it influences the size of the area of the drainage system. GHF also determines the water input and hence controls where the efficient drainage system activates. With a warming climate, an increase in surface runoff is expected, and higher velocities for the outlet glaciers of Greenland will lead to higher frictional heat and higher basal melt rates. Therefore, representing the area and efficiency of the hydrological system is crucial in order to predict the response of ice streams such as the NEGIS to future climate changes. High GHF produces a system with more developed efficient drainage systems and a domain that is mostly thawed. A system with high GHF may be less sensitive, and possibly be able to compensate for a higher water input. In this case an increase in water input will have a larger area over which to spread, and the system will be more efficient in evacuating water away giving a lower water pressure.

We show that effective pressure is an important control on the dynamics of the NEGIS. Future studies should include subglacial hydrology in the inversion process. In this way, less information will be hidden in the friction coefficient and assumed to be constant in time. Instead, basal friction may evolve with a changing climate through time. Future studies should therefore focus on coupling SMB models and subglacial hydrology models to account for changes in basal conditions as surface runoff varies. Additionally, a fully coupled hydrology and ice dynamics model would improve the feedbacks associated with velocity increases, leading to more water and in turn even higher velocities.

5. Conclusions

Effective pressure can account for a substantial part of the spatial variations in NEGIS velocities. Uncertainties in GHF dictate model representation of basal melt, effective pressure, and therefore the ice flow. A minimal GHF results in a domain where regions outside the main trunk are frozen to the bed with no subglacial hydrology. This is in contrast to the maximum GHF, where a substantial part of the bed is thawed, and the drainage system is more efficient. This implies that the GHF controls the sensitivity of the hydrology system and must be represented in order to characterize dynamical subglacial systems like that of the NEGIS. Ice flux uncertainties in the northeast sector of the GrIS, given uncertainties in GHF associated with sliding, are 10 times larger than those associated with ice viscosity. Overall, we find that GHF uncertainties introduce an uncertainty in ice discharge of 0.25 Gt/yr associated with viscosity, and 2.10 Gt/yr associated with effective pressure from the three main outlets of the NEGIS.

Acknowledgments
S. S. J., B. d. F., and K. H. N. were funded by the Ice2Ice project that has received funding from the European Research Council under the European Community's Seventh Framework Programme (FP7/2007-2013)/ERC Grant Agreement 610055. Funding for N. S. was provided by grants from NASA Cryospheric Science and Modeling, Analysis and Prediction (MAP) Programs. We gratefully acknowledge computational resources and support from the NASA Advanced Supercomputing Division. We thank Irina Rogozhina for providing the GHF map. We would also like to thank the three anonymous reviewers for greatly improving the manuscript.

Data Availability Statement

ISSM software is open source and can be downloaded at https://issm.jpl.nasa.gov/. The SMB forcing, errors, and components, used in this study are available from https://zenodo.org/record/3359192#.XUSmSpNKhR4 (Box, 2019). GHF map by Rogozhina et al. (2016) is available online (https://zenodo.org/record/3548190#.XdUEZ0N7mkA). GHF map by Martos et al. (2018) is available online (https://doi.pangaea.de/10.1594/PANGAEA.892973). GHF map by Greve (2019) is available online (https://doi.org/10.17592/001.2018022701). GHF map by Shapiro and Ritzwoller (2004) is available at online (http://ciei.colorado.edu/~nshapiro/MODEL/index.html). GHF map by Fox Maule et al. (2009) is available online (http://websrv.cs.umt.edu/isis/index.php/Greenland_Basal_Heat_Flux).

References

Aschwanden, A., Bueler, E., Khroulev, C., & Blatter, H. (2012). An enthalpy formulation for glaciers and ice sheets. *Journal of Glaciology*, *58*(209), 441–457.

Beyer, S., Kleiner, T., Aizinger, V., & Humbert, A. (2018). A confined unconfined aquifer model for subglacial hydrology and its application to the North East Greenland Ice Stream. *The Cryosphere Discussions*, *12*, 3931–3947.

Bindschadler, R. A., Nowicki, S., Abe-Ouchi, A., Aschwanden, A., Choi, H., Fastook, J., et al. (2013). Icesheet model sensitivities to environmental forcing and their use in projecting future sea level (the SeaRISE project). *Journal of Glaciology*, *59*, 195–224.

Box, J. E. (2013). Greenland ice sheet mass balance reconstruction. Part II: Surface mass balance (1840-2010). *Journal of Climate*, *26*(18), 6974–6989.

Box, J. E. (2019). Greenland monthly surface mass balance 1840–2012.

Church, J., Clark, P. U., Cazenave, A., Gregory, J. M., Jevrejeva, S., Levermann, A., et al. (2013). *Climate change 2013: The physical science basis, contribution of working Group I to the fifth assessment report of the intergovernmental panel on climate change Edited by* Stocker, T. F., Qin, D., Plattner, G.-K., Tignor, M., Allen, S. K., Boschung, J., Nauels, A., Xia, Y., Bex, V., & Midgley, P. M., Cambridge, United Kingdom and New York, NY, USA: Cambridge University Press.

Cuffey, K. M., & Paterson, W. S. B. (2010). *The physics of glaciers* (4th ed.). Oxford: Butterworth-Heinemann.

Cuzzone, J. K., Morlighem, M., Larour, E., Schlegel, N., & Seroussi, H. (2018). Implementation of higher-order vertical finite elements in ISSM v4.13 for improved ice sheet flow modeling over paleoclimate timescales. *Geoscientific Model Development*, *11*(5), 1683–1694.

de Fleurian, B., Gagliardini, O., Zwinger, T., Durand, G., Le Meur, E., Mair, D., & Räback, P. (2014). A double continuum hydrological model for glacier applications. *Cryosphere*, *8*(1), 137–153.

de Fleurian, B., Morlighem, M., Seroussi, H., Rignot, E., van den Broeke, M. R., Kuipers Munneke, P., et al. (2016). A modeling study of the effect of runoff variability on the effective pressure beneath Russell Glacier, West Greenland. *Journal of Geophysical Research: Earth Surface*, *121*, 1834–1848. https://doi.org/10.1002/2016JF003842

Doubrovine, P. V., Steinberger, B., & Torsvik, T. H. (2012). Absolute plate motions in a reference frame defined by moving hotspots in the Pacific, Atlantic and Indian oceans. *Journal of Geophysical Research*, *117*, B09101. https://doi.org/10.1029/2011JB009072

Eldred, M. S., Adams, B. M., Gay, D. M., Swiler, L. P., Haskell, K., Bohnhoff, W. J., et al. (2008). DAKOTA, A multilevel parallel object-oriented framework for design optimization, parameter estimation, uncertainty quantification , and sensitivity analysis version 4.2 Reference Manual. Tech. Rep SAND2006-6337, Sandia Natl. Lab., Albuquerque, N. M.

Ettema, J., Bales, R. C., Box, J. E., van Meijgaard, E., van den Broeke, M. R., van de Berg, W. J., & Bamber, J. L. (2009). Higher surface mass balance of the Greenland ice sheet revealed by high-resolution climate modeling. *Geophysical Research Letters*, *36*, L12501. https://doi.org/10.1029/2009GL038110

Fahnestock, M., Abdalati, W., Joughin, I., Brozena, J., & Gogineni, P. (2001). High geothermal heat flow, basal melt, and the origin of rapid ice flow in central Greenland. *Science*, *294*(5550), 2338–2342.

Fox Maule, C., Purucker, M. E., & Olsen, N. (2009). Inferring magnetic crustal thickness and geothermal heat flux from crustal magnetic field models. November.

GRIP (1993). Climate instability during the last interglacial period recorded in the GRIP ice core. *Nature*, *364*(6434), 203–207.

Glen, J. W. (1955). The creep of polycrystalline ice. *Proceedings of the Royal Society A*, *228*(1175), 519–538.

Greve, R. (2019). Geothermal heat flux distribution for the Greenland ice sheet, derived by combining a global representation and information from deep ice cores. *Polar Data Journal*, *3*, 22–63.

Hendrickson, B, & Leland, R (1995). The Chaco user's guide, version 2.0: Technical report, Sandia National Laboratories, Albuquerque, NM87185-1110.

Hindmarsh, R. C. A. (2004). A numerical comparison of approximations to the Stokes equations used in ice sheet and glacier modeling. *Journal of Geophysical Research*, *109*, F01012. https://doi.org/10.1029/2003JF000065

Howat, I. M., Negrete, A., & Smith, B. E. (2014). The Greenland Ice Mapping Project (GIMP) land classification and surface elevation data sets. *Cryosphere*, *8*(4), 1509–1518.

Keisling, B. a., Christianson, K., Alley, R. B., Peters, L. E., Christian, J. E. M., Anandakrishnan, S., et al. (2014). Basal conditions and ice dynamics inferred from radar-derived internal stratigraphy of the northeast Greenland ice stream. *Annals of Glaciology*, *55*(67), 127–137.

Larour, E., Morlighem, M., Seroussi, H., Schiermeier, J., & Rignot, E. (2012). Ice flow sensitivity to geothermal heat flux of Pine Island Glacier, Antarctica. *Journal of Geophysical Research*, *117*, F04023. https://doi.org/10.1029/2012JF002371

Larour, E., Seroussi, H., Morlighem, M., & Rignot, E. (2012). Continental scale, high order, high spatial resolution, ice sheet modeling using the Ice Sheet System Model (ISSM). *Journal of Geophysical Research*, *117*, F01022. https://doi.org/10.1029/2011JF002140

Martos, Y. M., Jordan, T. A., Catalan, M., Jordan, T. M., Bamber, J. L., & Vaughan, D. G. (2018). Geothermal heat flux reveals the Iceland hotspot track underneath Greenland. *Geophysical Research Letters*, *45*, 8214–8222. https://doi.org/10.1029/2018GL078289

Morlighem, M., Rignot, E., Mouginot, J., Seroussi, H., & Larour, E. (2014). Deeply incised submarine glacial valleys beneath the Greenland ice sheet. *Nature Geoscience*, *7*(6), 18–22.

NEEM (2013). Eemian interglacial reconstructed from a Greenland folded ice core. *Nature*, *493*(7433), 489–494.

NGRIP (2004). High-resolution record of Northern Hemisphere climate extending into the last interglacial period. *Nature*, *431*, 147–151.

Pollack, H. N., Hurter, S. J., & Johnson, J. R. (1993). Heat flow from the Earth's interior: Analysis of the global data set. *Reviews of Geophysics*, *31*(3), 267–280.

Rignot, E., Gogineni, S, Joughin, I., & Krabill, W. (2001). Contribution to the glaciology of northern Greenland from satellite radar interferometry. *Journal of Geophysical Research*, *106*, 34,007–34,019.

Rignot, E., & Mouginot, J. (2012). Ice flow in Greenland for the International Polar Year 2008-2009. *Geophysical Research Letters*, *39*, L11501. https://doi.org/10.1029/2012GL051634

Rogozhina, I., Hagedoorn, J. M., Martinec, Z., Fleming, K., Soucek, O., Greve, R., & Thomas, M. (2012). Effects of uncertainties in the geothermal heat flux distribution on the Greenland Ice Sheet: An assessment of existing heat flow models. *Journal of Geophysical Research*, *117*, F02025. https://doi.org/10.1029/2011JF002098

Rogozhina, I., Petrunin, A. G., Vaughan, A. P. M., Steinberger, B., Johnson, J. V., Kaban, M. K., et al. (2016). Melting at the base of the Greenland ice sheet explained by Iceland hotspot history. *Nature Geoscience*, *9*(5), 366–369.

Schlegel, N. J., & Larour, E. Y. (2019). Quantification of surface forcing requirements for a Greenland ice sheet model using uncertainty analyses. *Geophysical Research Letters*, *45*, 9700–9709. https://doi.org/10.1029/2019GL083532

Schlegel, N. J., Larour, E., Seroussi, H., Morlighem, M., & Box, J. E. (2013). Decadal-scale sensitivity of Northeast Greenland ice flow to errors in surface mass balance using ISSM. *Journal of Geophysical Research: Earth Surface*, *118*, 667–680. https://doi.org/10.1002/jgrf.20062

Schlegel, N.-J., Larour, E., Seroussi, H., Morlighem, M., & Box, J. E. (2015). Ice discharge uncertainties in Northeast Greenland from climate forcing and boundary conditions of an ice flow model. *Journal of Geophysical Research: Earth Surface*, *120*, 29–54. https://doi.org/10.1002/2014JF003359

Schlegel, N. J., Seroussi, H., Schodlok, M. P., Larour, E. Y., Boening, C., Limonadi, D., et al. (2018). Exploration of Antarctic Ice Sheet 100-year contribution to sea level rise and associated model uncertainties using the ISSM framework. *Cryosphere*, *12*(11), 3511–3534.

Schlegel, N.-J., Wiese, D. N., Larour, E. Y., Watkins, M. M., Box, J. E., Fettweis, X., & van den Broeke, M. R. (2016). Application of GRACE to the evaluation of an ice flow model of the Greenland Ice Sheet. *The Cryosphere Discussions*, *2016*, 1–35.

Seroussi, H., Morlighem, M., Rignot, E., Khazendar, A., Larour, E., & Mouginot, J. (2013). Dependence of century-scale projections of the Greenland ice sheet on its thermal regime. *Journal of Glaciology*, *59*(218), 1024–1034.

Shapiro, N. M., & Ritzwoller, M. H. (2004). Inferring surface heat flux distributions guided by a global seismic model: Particular application to Antarctica. *Earth and Planetary Science Letters*, *223*(1-2), 213–224.

Storey, M., Duncan, R. A., & Tegner, C. (2007). Timing and duration of volcanism in the North Atlantic Igneous Province: Implications for geodynamics and links to the Iceland hotspot. *Chemical Geology*, *241*(4), 264–281.

Swiler, L. P., & Wyss, G. D. (2004). A user's guide to Sandia's Latin hypercube sampling software: LHS UNIX Library/Standalone Version, Technical Report SAND2004-2439. Sandia National Laboratories.

van den Broeke, M., Bamber, J. L., Ettema, J., Rignot, E., Schrama, E., van de Berg, W. J., et al. (2009). Partitioning recent Greenland mass loss. *Science*, *326*, 984–986.